

## **Experimental study on seismic wave velocity of hydrate-bearing fine-grained sediments**

Hak-Sung Kim<sup>1)</sup>, Tae-Hyuk Kwon<sup>2)</sup>, and \*Gye-Chun Cho<sup>3)</sup>

<sup>1), 3)</sup> *Department of Civil and Environmental Engineering, KAIST, Daejeon 305-701,  
Korea*

<sup>2)</sup> *Department of Civil and Environmental Engineering,  
Washington State University, Pullman, Washington, U.S.A.*

<sup>3)</sup> [gyechun@kaist.edu](mailto:gyechun@kaist.edu)

### **ABSTRACT**

Synthesizing gas hydrate in a fine-grained natural seabed sediment sample, mainly composed of silty-to-clayey soils, has been hardly attempted due to the low permeability. It has been known that hydrate loci in pore spaces and heterogeneity of hydrate growth in core-scale play a critical role in determining physical properties of hydrate-bearing sediments. In the presented study, we attempted to identify the effect of hydrate growth morphology on seismic velocities in natural fine-grained sediments sampled from the Ulleung Basin in East Sea. We synthesized CO<sub>2</sub> hydrate in clayey silt sediments in an instrumented oedometric cell and measured seismic velocities during hydrate formation and loading processes. Herein, we present the experiment results on P-wave and S-wave velocities of gas hydrate-bearing fine-grained sediments. It is found that geophysical properties of gas hydrate-bearing sediments are governed by hydrate saturation and effective stress as well as morphological feature of hydrate formation in sediments.

---

<sup>1)</sup> Graduate Student

<sup>2)</sup> Assistant professor

<sup>3)</sup> Professor

## 1. INTRODUCTION

Methane hydrate, the most common type occurring in nature, has been found in both permafrost sediments to depth of about 1 km and deep marine sediments at water depth greater than about 300m in continental margins. The vast amounts of gas hydrate reserves have drawn scientific attentions as a potential energy resource.

Meanwhile, CO<sub>2</sub> hydrate could provide sealing capacity in underground storage of CO<sub>2</sub> by its self-trapping mechanism (Koide et al., 1995). CO<sub>2</sub> hydrate is stable at seafloor with low temperature gradient. The CO<sub>2</sub> sequestration in deep marine sediments using CO<sub>2</sub> hydrate has a large potential on carbon capture and storage (CCS) because it does not require cap-rock structure on the permeable layer. Cost effectiveness, large storage capacity and flexibility could be provided by this storage method (House et al., 2006; Koide et al., 1997; Rochelle et al., 2009; Tohidi et al., 2010). When liquid or supercritical CO<sub>2</sub> is injected into the ocean-bottom, permafrost, or deep-lake sediments below the CO<sub>2</sub> hydrate stability zone (e.g., temperature < 10°C, pressure > 5 MPa), the CO<sub>2</sub> is transported upward to the hydrate stability zone by buoyancy-driven convection, and subsequently forms hydrate. It has also been observed in a laboratory environment that CO<sub>2</sub> hydrate can accumulate and occupy ~90% of pore spaces in a sandy sediment within 12 hours, purely by molecular diffusion (Kwon and Cho, 2009). Thus, a CO<sub>2</sub> hydrate-forming reservoir could provide a secondary seal independently, and, as such, CO<sub>2</sub> hydrate-based sequestration technology is a very attractive alternative to conventional technology, which relies on natural geological seals.

Geophysical properties of hydrate-bearing sediments, such as elastic wave velocities and electrical resistivity, are important to monitor during methane production from hydrate-bearing deposits and during CO<sub>2</sub> hydrate formation in CO<sub>2</sub>-injected deposits (Kwon and Cho, 2009). And these properties could be used as essential input parameters for numerical simulations of gas hydrate production and CO<sub>2</sub> sequestration using CO<sub>2</sub> hydrate.

Although host sediments containing natural gas hydrates have been reported to be mostly fine-grained sediments, synthesizing gas hydrate in fine-grained sediments in laboratory has been considered as challenges due to its low permeability and innate heterogeneity when forming gas hydrate in core-scale (Lee et al., 2010). In addition, few geophysical characterizations have been made particularly for natural deep sediments cored from the Ulleung Basin. We have performed laboratory experiments on CO<sub>2</sub> hydrate-bearing sediments using a sediment sample cored from a hydrate occurrence region in the Ulleung Basin, East Sea, offshore Korea. In this paper, measured seismic wave velocities are presented, and the effects of hydrate saturation and effective stress on the seismic velocities are discussed.

## 2. EXPERIMENTAL PROGRAM

### 2.1 Description of Sediment Sample

The Ulleung Basin is located in the southwestern part of the East Sea. It is a deep, bowl-shaped and back-arc basin. The water depth of the basin ranges from 1500 to

2300 m (Lee and Kim, 2002). The sediment sample recovered from UBGH1-10, where gas hydrates were found to occur between seafloor and 141 mbsf (Kwon et al., 2011), was chosen for this study. The sample was cored from the depth of 121 mbsf. Index properties of the sediment sample are summarized in Table 1. The sample is characterized by high plastic silty soil (i.e., MH by USCS distinction), and has a fairly high specific surface area of 98 m<sup>2</sup>/g.

## 2.2 Test Setup

The test setup was designed to synthesize CO<sub>2</sub> hydrate in sediments and to measure geotechnical and geophysical properties. All the experiments were conducted in a cylindrical, rigid-wall high pressure cell (i.e., volume of 160.8 cm<sup>3</sup>; internal diameter of 66 mm; internal height of 140 mm) instrumented to measure temperature, pressure, P-wave, S-wave, electrical resistivity, and vertical displacement (Fig. 1). Effective stress, which is an overburden pressure to the soil skeleton, was applied by a loading plate, the force of which was controlled by an external air cylinder. The cell hosted one T-type thermocouple for measuring the temperature of the specimen interior, one pressure transducer for pressure, one pair of bender elements for shear wave (S-wave) measurement, one pair of piezo-plates for compressional wave (P-wave) measurement, and one pair of electrodes for electrical resistivity measurement.

The temperature of the high pressure cell was controlled by circulating temperature-controlled fluids from a refrigerating circulator through a copper tube coiled around the cell. 5 mm-long bender elements were used for S-wave measurement, while 10 mm-diameter PZT plates were used for P-wave measurements. Square-shaped signals with 10 volts were used as excitation, and the input frequency ranged from 1 kHz to 10 kHz.

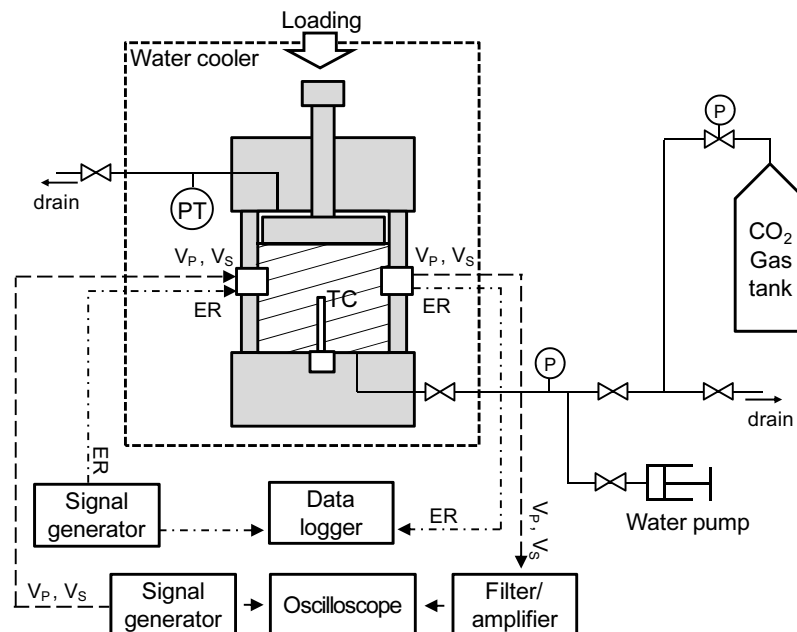


Fig. 1 Schematic drawing of experimental setup ( $V_p$ : PZT plate,  $V_s$ : bender elements, ER: electrode, PT: pressure transducer, TC: thermocouple).

Table 1. Description and index properties of the sediment sample tested.

| PL (%) | LL (%) | Specific gravity | USCS | Mean particle size ( $\mu\text{m}$ ) | Specific Surface area ( $\text{m}^2/\text{g}$ ) |
|--------|--------|------------------|------|--------------------------------------|-------------------------------------------------|
| 46     | 62     | 2.52             | MH   | 9.4                                  | 98                                              |

### 2.3 Experimental procedure

The sediment sample was desalinated by distilled water to remove the effect of salinity on hydrate formation. The sample was partially saturated (water saturations of 28, 47, and 63%) with distilled water to control gas hydrate saturation. After compacting the sample into the cell, an effective vertical stress of  $\sim 100$  kPa was applied. The partially water-saturated specimen was cooled down to about  $1\text{--}2^\circ\text{C}$  at a constant pressure of  $\sim 2.75$  MPa to form hydrate in the specimen. After hydrate nucleation, the sample was kept in the same condition while supplying  $\text{CO}_2$  gas and maintaining pressure until no further hydrate formation was indicated by geophysical signatures. More than 24 hours were given for a specimen to be stabilized. Nitrogen ( $\text{N}_2$ ) gas was injected to flush  $\text{CO}_2$  gas in pores of sediments and tubes of the testing system to avoid additional  $\text{CO}_2$  hydrate formation. Then, distilled water was introduced to water-saturate the specimen and simulate the oceanic hydrate condition without free gas phase in pores. A loading process by increasing vertical effective stress was applied while pressure, temperature vertical displacement, seismic wave velocities and electrical resistivity were measured. This procedure was repeated for different water saturations, thus for resulted hydrate saturations of 28%, 47%, and 63%.

## 3. RESULTS AND DISCUSSION

### 3.1 Hydrate formation

Fig. 2 shows the evolution of pressure, temperature, electrical resistivity, and elastic wave velocities during the hydrate formation process and the post-water saturation process for the specimens with hydrate saturations ( $S_H$ ) of 63%. As the temperature decreases, hydrate formation was started with a temperature jump by an exothermic reaction, gradual increases in elastic wave velocities (P-wave, S-wave) and electrical resistivity. It was observed that hydrate formation stiffened host sediments and increased elastic wave velocities. Because forming hydrate crystals reduced free-electron passage in porous media, a decrease in electrical resistivity of the sediment was observed.

The geophysical signatures ( $V_P$ ,  $V_S$ , and electrical resistivity) show a gradual increase within a time scale of tens of hours, suggesting that the hydrate forms gradually throughout the specimen rather than instantly. For  $S_H = 63\%$ , it took  $\sim 10$  hours for  $V_P$  and  $V_S$  to reach plateaus (Fig. 2c, 2d). The amplitude of the exothermic temperature jump and the time for the temperature of the specimen interior to stabilize and reach equilibrium also support this gradual hydrate formation. However, the

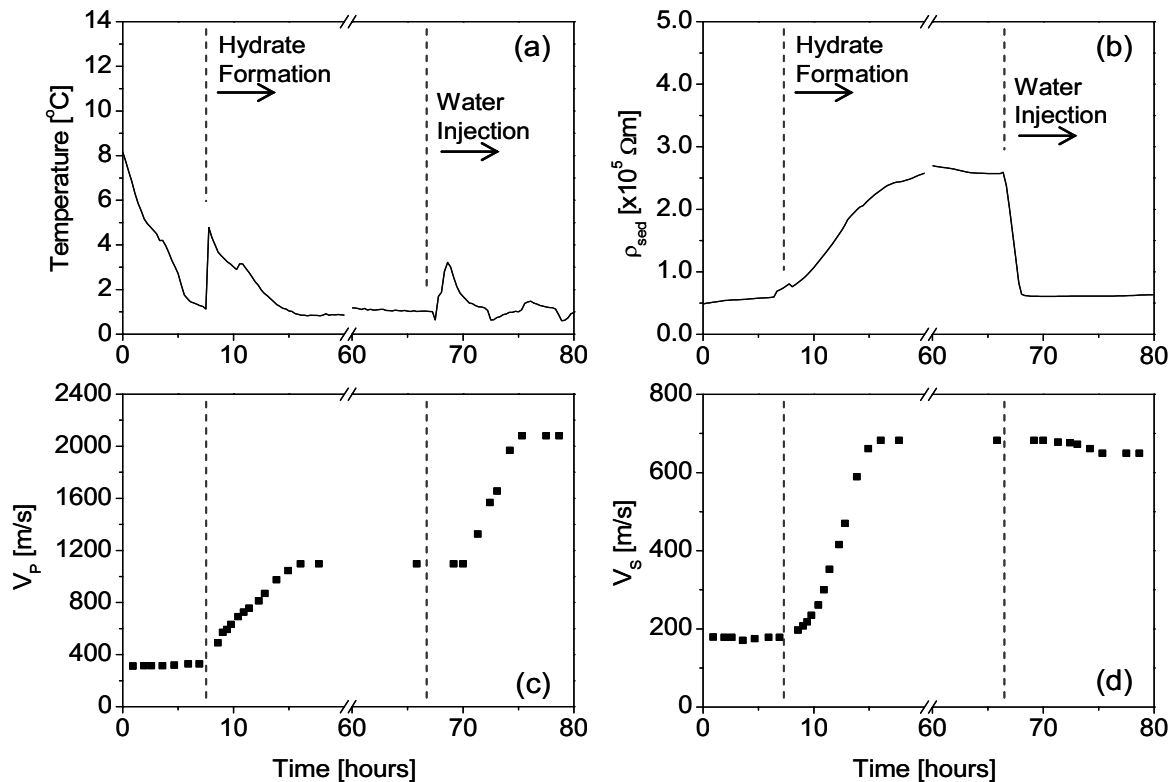


Fig. 2 Evolution of (a) temperature, (b) electrical resistivity ( $\rho_{\text{sed}}$ ), (c) P-wave velocity ( $V_P$ ), and (d) S-wave velocity ( $V_S$ ) of the sediment sample during hydrate formation and water saturation processes, under the vertical effective stress of 100 kPa. The results are from the test targeting for initial hydrate saturation of 63%.

electrical resistivity hardly supports the gradual hydrate growth, as shown in Fig. 2b. It is because electrical resistivity can be significantly affected by the local blockage of electron passages, e.g., if even a small amount of local hydrate formation happens to surround an exposed electrode that acts as a receiver or a source, it would lead to a huge increase in electrical resistivity.

During the water-saturating process, P-wave velocity increased and electrical resistivity decreased. A temperature jump by  $\sim 4^\circ\text{C}$  occurred because the injected water was relatively warmer than the sediment in the cell. Nevertheless, it is expected that additional hydrate formation or dissolution was insignificant, because, S-wave velocity was nearly unchanged during and after water injection.

### 3.2 Loading Process

Fig. 3 shows evolution of seismic wave velocities during a loading process where the vertical effective stress increases from 0.1 to 2.5 MPa. In general, P-wave velocity was observed to be less dependent on vertical effective stress and more sensitive to hydrate saturation. It is because P-wave propagation is mostly governed by properties

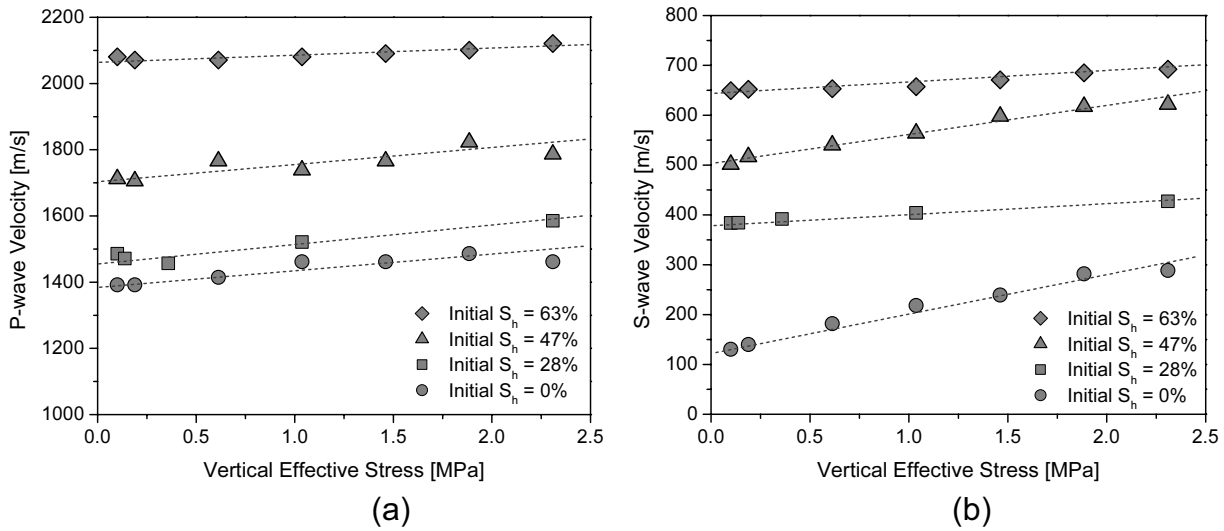


Fig. 3. Elastic wave velocities of gas hydrate-bearing sediment samples with different gas hydrate saturations during loading processes. (a) P-wave velocity, and (b) S-wave velocity.

and composition of pore-filling fluids. S-wave velocity showed larger dependency on the vertical effective stress than P-wave velocity did.

It was observed that the effect of vertical effective stress on elastic wave velocity decreased with increasing hydrate saturation. It indicates that higher hydrate saturation induces larger cementation effect between grains, such that it diminishes the stress-dependency of the sediment stiffness. At the hydrate saturation of 63%, the P-wave and S-wave velocities were nearly influenced by the increase of vertical effective stress in the tested range (i.e., 0 to 2.5MPa). This may reflect skeletal stiffening mechanism of hydrate-bearing sediments alternated from pore-filling to load-bearing or cementation at the hydrate saturation regime of ~63% (Waite et al., 2007).

### 3.2 Effect of hydrate formation on seismic wave velocity

Fig. 4 shows the effect of hydrate saturation on seismic velocity under the vertical stress of 1 MPa. It has been reported that the pore-filling mechanism is dominant in low hydrate saturation regime (e.g., < 40%) in coarse-grained sediments, after then load-bearing mechanism and cementation mechanism prevail in high saturation regime (Lee et al., 2010; Yun et al., 2005). However, the results shown in this study implies the transition to pore-filling morphology to cementing mechanism would occur at lower hydrate saturation (i.e., < 30%). Due to the innate nature of heterogeneous hydrate formation by small pores in fine-grained sediments, the possibility of localized hydrate formation, such as lens and veins, cannot be excluded.

Experiment results are compared with the models suggested by Lee et al. (2010) as shown in Fig. 4. The model was developed based on the measurements on fine-grained sediments (silt and clay) containing high hydrate saturations (50% and 100%).

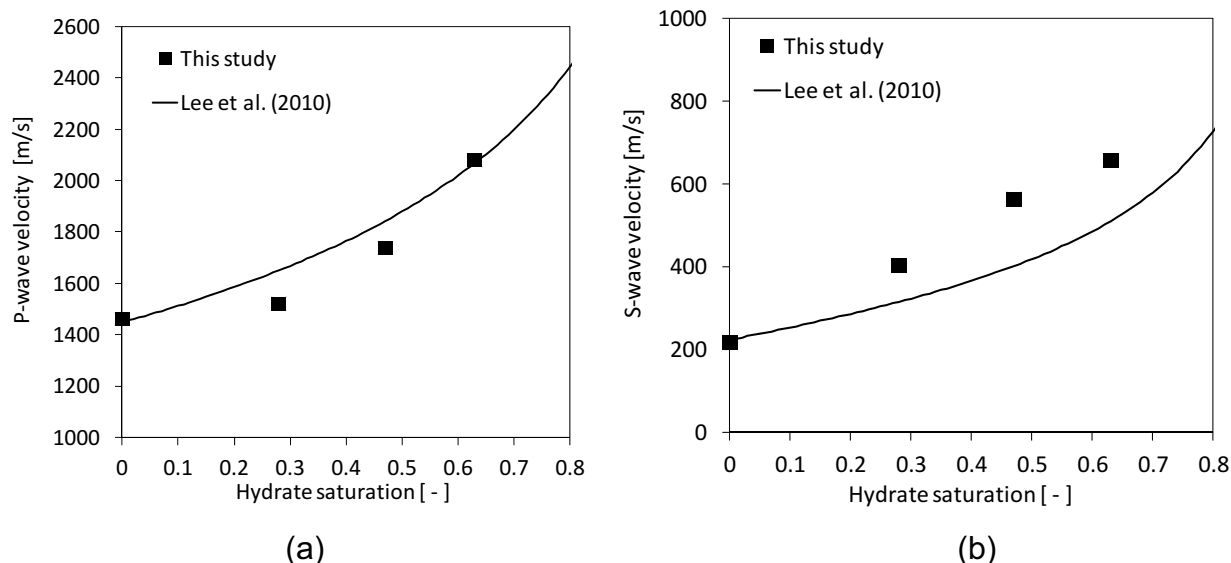


Fig. 4. Seismic wave velocities with gas hydrate saturation at the vertical effective stress of 1.3 MPa (a) P-wave velocity (b) S-wave velocity. Note that in the  $V_S$  model by Lee et al.(2010), we used  $\alpha = 47.92$ ,  $\beta = 0.13$ ,  $\sigma_v = 1.3\text{MPa}$ ,  $\sigma_h = 0.6\text{MPa}$ ,  $\theta = 0.13$ ,  $V_h = 1633\text{ m/s}$ , and  $n = 0.67$ . For  $V_P$  model by Lee et al. (2010),  $B_w = 2.5\text{ GPa}$ ,  $B_{\text{hyd}} = 5.6\text{ GPa}$ ,  $B_{\text{mineral}} = 36\text{ GPa}$ ,  $\rho_{\text{mix}} = 1550\text{ kg/m}^3$  and  $v_{\text{sk}} = 0.1$  were used.

In this study, however, the sediment containing hydrate saturation of ~30% showed faster  $V_S$  than the model predicts. Given that heterogeneous hydrate formation can be more severe in low saturation regime, it implies that models considering uniform hydrate formation and distribution may find difficulty to apply for fine-grained sediments containing hydrate less than 50%.

## CONCLUSIONS

This study presents geophysical measurements conducted on a clayey-silt sediment containing  $\text{CO}_2$  hydrate with different hydrate saturations and under different vertical effective stresses. The objective of this study is to identify seismic wave velocity characteristics of hydrate-bearing fine-grained sediments cored from Ulleung Basin, East sea, offshore Korea.

Seismic waves of hydrate-bearing sediments are found to be controlled by hydrate saturation and effective stress. Hydrate saturation showed significant impacts on elastic wave velocities. Effect of vertical effective stress on elastic wave velocities decreased with increasing hydrate saturation. Hydrate morphology transition from pore-filling mechanism to load-bearing and cementation mechanism is assumed to take place in the hydrate saturation less than 30%. Cementation effect may be enhanced by localized gas hydrate formation in fine-grained sediments.

## ACKNOWLEDGEMENTS

This research was supported by a grant from the National Research Foundation of Korea (NRF) funded by the Korean government (MEST) (No. 2011-0027591) and by the Basic Research Project of the Korea Institute of Geoscience and Mineral Resources(KIGAM) funded by the Ministry of Knowledge Economy of Korea.

## REFERENCES

- House K.Z., Schrag D.P., Harvey C.F., and Lackner, K.S. (2006). "Permanent carbon dioxide storage in deep-sea sediments", *Proceedings of the National Academy of Sciences(PNAS)*, Vol. **103**(33), 12291-12295.
- Koide, H., Takahashi, M., Ysukamoto, H., and Shindo, Y. (1995), "Self-trapping mechanisms of carbon dioxide in the aquifer disposal", *Energy Conversion and Management*, Vol. **26**, No.6-9, pp.505-508.
- Koide, H., Takahashi, M., Shindo, Y., Tazaki, Y., Iijima, M., Ito, K., Kimura, N., and Omata, K. (1997), "Hydrate formation in sediments in the sub-seabed disposal of CO<sub>2</sub>", *Energy*, Vol. **22**, pp.279-283.
- Kwon T.H., and Cho G.C. (2009). "Evolution of Compressional wave velocity during CO<sub>2</sub> hydrate formation in sediments". *Energy and Fuels* Vol. **23**(11), 5731-5736.
- Kwon T.H., Lee K.R., Cho G.C., and Lee J.Y. (2011). "Geotechnical properties of deep oceanic sediments recovered from the hydrate occurrence regions in the Ulleung basin, East Sea, offshore Korea", *Marine and Petroleum Geology*, Vol. **28**, Issue 10, pp.1870-1883.
- Lee, K.W., and Kim, B. (2002). "Infill history of the Ulleung basin, East Sea (Sea of Japan) and implications on source rocks and hydrocarbons", *Marine and Petroleum Geology* Vol. **19**, 829-845.
- Lee, J.Y., Francisca, F.M., Santamarina, J.C., Ruppel, C., (2010) "Parametric study of the physical properties of hydrate-bearing sand, silt, and clay sediments: 2.small-strain mechanical properties", *Journal of Geophysical Research* 2010; **115**, B11105, doi:10.1029/2009JB006670.
- Rochelle, C.A., Camps, A.P., Long, D., Mildowoski. A., Bateman, K., Gunn, D., Jackson, P., Lovell, M.A., Rees, J. (2009), "Can CO<sub>2</sub> hydrate assist in the underground storage of carbon dioxide?", *Geological Society, London, Special Publications, 2009*, 319:171-183, doi:10.1144/SP319.14.
- Tohidi, B., J. H. Yang, M. Salehabadi, R. Anderson, and A. Chapoy. (2010). "CO<sub>2</sub> Hydrates Could Provide Secondary Safety Factor in Subsurface Sequestration of CO<sub>2</sub>", *Environmental Science & Technology*, Vol. **44**, 1509-1514.
- Yun, T.S., Francisca, F.M., Santamarina, J.C., Ruppel, C. (2005), "Compressional and shear wave velocities in uncemented sediment containing gas hydrate", *Geophysical Research Letters* 2005; **32**, L10609, doi:10.1029/2005GL022607.